Journal homepage www.jzs.univsul.edu.iq
Journal of Zankoy Sulaimani
Part-A- (Pure and Applied Sciences)

Adsorptive removal of methyl orange from aqueous solutions with natural Garmak clay as cheap and efficient adsorbent in batch and continuous systems

Karukh Ali Babakr[1,2*] and Bakhtyar Kamal Aziz[3]

[1]*Chemistry department, College of Science, University of Raparin, Rania-Sulaimani, Iraq, 46012.*
**karukh.ali@raparinuni.org*
[2]*Chemistry Department, College of Science, University of Sulaimani, Sulaimani, Iraq, 46001.*
[3]*College of Medicals and Applied Sciences, Charmo University, Chamchamal-Sulaimani, Iraq, 46025*
bakhtyar.kamal@charmouniversity.org

Article info

Original: 1 September 2019
Revised: 25 October 2019
Accepted: 17 November 2019
Published online: 20 December 2019

Key Words:
Local clay
Adsorption
Non-linear regression
Fixed bed

Abstract

The natural clay of North Garmak-Sulaimani was characterized with XRF, XRD and FTIR. The specific surface area (18.8 m^2 g^{-1}) was determined with N_2 gas adsorption analyzer using multi-point BET isotherm and 0.054 cc g^{-1} total pore volume. The cation exchange capacity was estimated as 12.4 mmol/100 g of the natural clay by the method of Cu-triene complex. The efficiency of the natural clay was evaluated for the adsorption of a model anionic dye (methyl orange) in batch system. Non-linear curve fitting was used to examine the kinetic and equilibrium experimental data for appropriate model. Langmuir, Freundlich and Temkin isotherms were fitted well to the experimental data. The best fit was with Langmuir model with a monolayer adsorption capacity of 63.9 mg g^{-1} at 30 ^oC. The kinetic data were best fit with pseudo second-order model. The thermodynamic parameters confirmed a spontaneous endothermic adsorption process. To bring the study to industrial scale, clay granules was made from the natural clay powder and used as fixed bed adsorbent in a column for continuous system. The operational conditions were optimized. Thomas kinetic model was found to fit the experimental kinetic data.

Introduction

Anomalous presence of many organic and inorganic compounds in industrial wastewater in developed countries became one of the most important environmental issue in the current century [1]. Among organic pollutants, dye stuff contributes to a great extent. The consumption of dyes in textile industries worldwide exceeded 10.000 tones/years and the discharging in to water stream is more than 100 tones/year [2]. Methyl orange (MO), a water soluble anionic dye is extensively used in textile, paper manufacturing, food, printing and pharmaceutical industries [1]. MO considered as hypersensitive material if swallowed, causes illness and even be shin eczema exhibition at contacting with skin [3].

Several techniques regarded as treatment/remove and adsorption of dyes have been used such as electro-coagulation, advanced oxidation processes, photo-degradations, and adsorption by active carbon [4]. Adsorption is an important technique used for the purification of influent media through separation and accumulation of dissolved compounds at the surface or into the interphase of a solid adsorbent [5]. In literature, different type of agricultural waste used as adsorbent for purification and removing of dyes from wastewater such as apple pomace and wheat straw [6], banana stalk [7], oil palm ash [8], pine tree leaves [9], rice husk [10], canola hull [11]. Now a day, using soil materials as adsorbent in purification became attracted to replace commercial adsorbents due to their low cost, abundancy, high surface area, ability for ion exchange, and environmentally save [12]. Clays has hydrous aluminosilicate composition of fine-grained clay minerals, crystals and metal oxides. Many types of clay are announced like smectites (montmorillonite, saponite), mica (illite), kaolinite, vermiculite, serpentine, pyrophyllite (talc), and sepiolite. The small particle

size and porous texture of clay material allows physicochemical interaction with dissolved species [13]. Surface properties of the clay and chemical properties of the molecules control the adsorption capacity of organic molecules on the clay [14].

In the present study, natural Garmk clay (NGC) was used as a cheap adsorbent to examine its effectiveness to remove MO from aqueous solution. The influence of operational parameters (pH, amount of clay, initial MO concentration) were investigated. The kinetic and equilibrium studies were performed to estimate the mechanism of the adsorption in batch system. To bring the study to industrial scale, the granules of Garmk clay (NGG) was prepared and used in fixed bed system to removal MO from wastewater. The effect of operational parameters was for the continuous system were carried out also.

Materials and Methods

A. Materials

Analytical grade Methyl Orange (Chemical formula $C_{14}H_{14}N_3NaO_3S$; molecular weight 327.33 g $mole^{-1}$) powder was obtained from Fluka (Figure:1). The Stock solution of MO was prepared by dissolving a known weight of the dye in distilled water. Other required dye series solutions were prepared by dilution from the stock solution. The calibration curve between absorbance (λ= 470 nm) vs standard concentrations of MO was obtained using UV-Visible spectrophotometer. Dilute HCl and NaOH solutions were used to adjust the initial solution pH.

The natural clay sample was taken under 50 cm from the surface of Garmk-Sulaimaini- Iraq. The fine particles of the natural clay were separated from the bulk by successive dilution and sedimentation in 1L cylinder. The fine fraction of the sample was dried at 105^{o}C and crushed with agate mortar then passed through 200 μm sieve. The product was assigned as natural Garmk clay (NGC) and kept in glass bottles to be used in batch adsorption experiments.

The clay granules (NGG) were prepared by mixing NGC with a limited amount of distilled water to prepare a clay paste that is suitable to pass through a 12 mesh sieve to make clay granules. Then the wet clay granules left for 24 hours at room temperature to obtain dry granules. Calcination of the granules was done at (450, 550, 650, 750 ^{o}C) for 4 hours. Different granule size was separated using different sieve sizes. The smallest granule size was obtained by crashing after calcination and passing suitable a sieve.

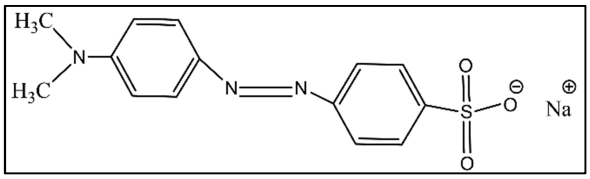

Figure-1: The chemical structure of methyl orange

B. Characterization of NGC

The chemical composition of NGC was determined using XRF with a PANalytical Axios spectrometer (ALMELO, The Netherlands). Gas adsorption analyzer (Quantachrome, AUTOSORBE-iQ-c) was used to measure the surface area and porosity of NGC. The sample was degassed at 473 K for 20h. The clay mineral faces and mineralogy was investigated with X-ray diffraction (XRD) technique. PANalytical X"Pert PRO MPD θ-θ diffractometer (Cu-$K_{\alpha 1}$ radiation generated at 40 kV and 30 mA) was used over the range (2θ= 0-40^o). The clay specimen was prepared by top-loading method. The clay suspension was deposited on circular 2.4 cm porous ceramic tiles. The mid-infrared spectra was recorded with Thermo Nicolet Nexus FTIR spectrometer. The KBr pellet technique (1 mg sample/200 mg KBr) was used.

C. Batch adsorption Studies

All batch adsorption experiments were carried out in 100 mL poly ethylene bottles using 0.1 gm of NGC and 50 mL of desired concentration of MO solution. After mixing, the mixtures were agitated in a thermostat water-bath shaker to specified times depending on the adsorption study. After specified time elapsed, 15 mL of the dispersions were centrifuged at 4500 rpm for 10 minutes and the concentration of the remained MO in

the solution (C_e) was measured using (Cary 60 UV-Vis spectrophotometer from Agilent Technologies) at λ_{max} = 507 nm. The amount of MO (q_e) adsorbed on NGC was calculated according to (Eq. 1).

$$q_e = \frac{(C_o - C_e)V}{m} \quad (1)$$

Where, C_o and C_e are the initial and equilibrium concentrations of MO (mg L^{-1}). V is the solution volume (L) and m is the adsorbent dose (g).

The equilibrium time of adsorption was investigated from the plot of q_e verses the contact time using 0.1 g of NGC and 50 mL solution of MO (100 mg L^{-1}). The equilibrium time study was repeated for various temperatures.

The effect of initial pH was carried out in the range of 3-9. NGC dosage study was performed to determine the effect of clay dose on the adsorption capacity of adsorbent. Various initial concentration of MO solution, ranging from 10 to 150 mg L^{-1} have been used to study the effect of initial concentration.

D. Fixed-bed adsorption studies

Granules of NGC were packed in a vertical glass column of 0.8 mm diameter. A small piece of glass wool was fixed at the top and the bottom of the column to prevent the elution of the granule particles. MO solution pumped out from the column using (chromatographic pump) to regulate the rate of solution flow. Every 5 minutes, the remained concentration (C_t) was determine using UV-Vis spectrophotometer.

The breakthrough curves were obtained from the plots of C_t or C_t/C_o vs eluted volume (mL) or elution time (min). The effect of calcining temperature of the clay granules was investigated using various calcination temperatures (450, 550 and 750^{o}C).

The effects of operational conditions (granule particle size, flow rate, MO concentration and bed height) were carried out to determine their influence on the adsorption capacity of the column.

E. Fixed-bed data analysis

Breakthrough can be investigated from C_t or Ct/C_o vs V_{eff} (mL) or t (min) plots. Where V_{eff} is the treated volume of effluent solution. V_{eff} could be determine as (Eq. 2):

$$V_{eff} = Qt \quad (2)$$

Where Q is influent flow rate (mL min^{-1}) and t is consumption time (min).

The adsorption capacity (mg) (q_{total}) could be determine by the computational determination of the area under the curve. achieved from the integration of MO concentration which adsorbed by adsorbent and expressed as C_{ad} (C_o-C_t) at a specified time can be calculated as in (Eq. 3):

$$q_{total} = \frac{QA}{1000} = \frac{Q}{1000}\int_{t=0}^{t_{total}} C_{ad}\,dt \quad (3)$$

Where A is the area under the plot, t_{total} is the total flow time. The equilibrium uptake q_e (mg g^{-1}) can be calculated from (Eq. 4):

$$q_{e(exp.)} = \frac{q_{total}}{m} \quad (4)$$

The amount of adsorbed MO from the NGG bed in the column (W_{total}) can be determine from (Eq. 5):

$$W_{total} = \frac{C_o Q t_{tptal}}{1000} \quad (5)$$

The percentage of adsorbed MO in the column were determined as $R\%$ (Eq. 6):

$$R\% = \frac{q_{total}}{W_{total}} \times 100 \quad (6)$$

F. Error analysis

The regression curves of the isotherm and kinetic models with the experimental data were tested by two methods of error analysis for non-linear regression. R^2 is the correlation coefficient by (Eq. 7) could be used to measure the correlation of experimental data with the isotherm and kinetic models.

$$R^2 = 1 - \frac{\Sigma(q_{exp} - q_{fit})^2}{\Sigma(q_{exp} - q_{mean})^2} \quad (7)$$

Where q_{exp} is the experimental data of the amount adsorbed, q_{fit} is the computed value of q_{exp} for the fitting curve and q_{mean} is the average of q_{exp}.

The second method for error analysis is the sum of square residual (*SSE*), as given in (Eq. 8). The smaller value of *SSE* confirms the better fit of the models with experimental data.

$$SSE = \sum(q_{exp} - q_{fit})^2 \qquad (8)$$

Result and Discussion

A. *Characterization of adsorbent NGC*

(**Error! Reference source not found.**) shows the chemical composition of clay. XRF values of chemical composition showed the major constituents was composed of SiO_2 and Al_2O_3 with smaller amounts of other presented constituents. XRD analysis were performed for the oriented slides for normal, air dried and ethylene glycol (EG) saturated mounts (Figure: 2). The main peak at 2θ= 26.6° is characteristic for quartz SiO_2 in the crystalline structure of the clay. The peak at 2θ=12.2° and 2θ= 2.0° are characteristic for kaolinite clay mineral (1st and 2nd order), respectively. Peaks at 2θ= 9.2° and 2θ= 18.2°, indicate the presence of Muscovite. The other 2θ= 6.0° reflection could be assigned to the presence of vermiculite clay minerals (limited expansion on EG saturation).

Table-1: The chemical composition of NGC represented as % of oxides

SiO_2	Al_2O_3	Fe_2O_3	MnO	MgO	Na_2O	K_2O	P_2O_5	TiO_2	CaO	LOI
52.58	22.72	8.03	0.16	2.02	0.67	4.12	0.13	1.00	0.80	7.53

The mid infrared spectra is shown in (Figure: 3) The band at 3699.96 cm^{-1} assigned to Al-OH stretching. Although, the band at 3622.48 cm^{-1} were assigned to muscovite. The later band at 3385.5 and 1636.8 cm^{-1} are characteristics of the H-O-H stretching and bending of adsorbed water. The bands at 1430.0, 796.8 and 694.9cm^{-1} are assigned to Si-O stretching and presence of quartz. The band at 1027 cm^{-1} assigned to the Si-O stretching of all silicates present in the sample.

From the N_2 adsorption experiments using gas adsorption analyzer, the specific surface area was measured using Brunauer-Emmet-Teller (BET) multi-point isotherm (SBET) as18.8 $m^2\ g^{-1}$ and the total pore volume of = 0.054 cc g^{-1} calculated at a relative pressure P/P_o of 0.992. The CEC was estimated as 12.4 mmol/100 g as measured by the Cu-trien method.

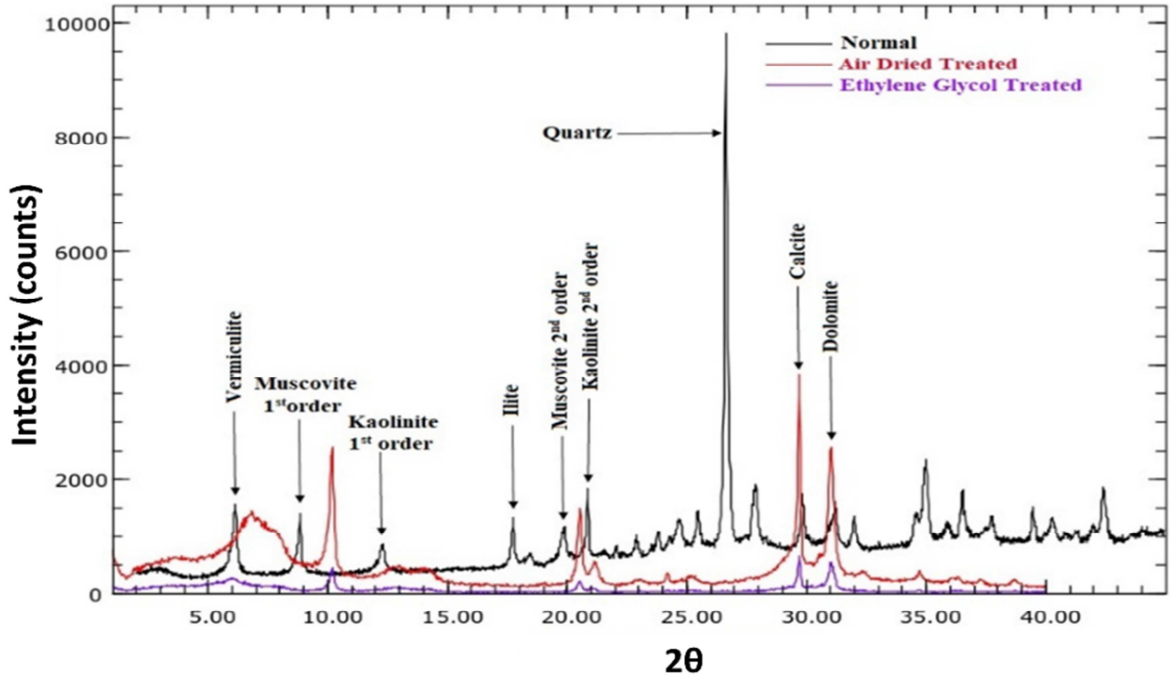

Figure-2: The XRD patterns of the natural NGC (black), air dried (red) and ethylene glycol saturated (violet)

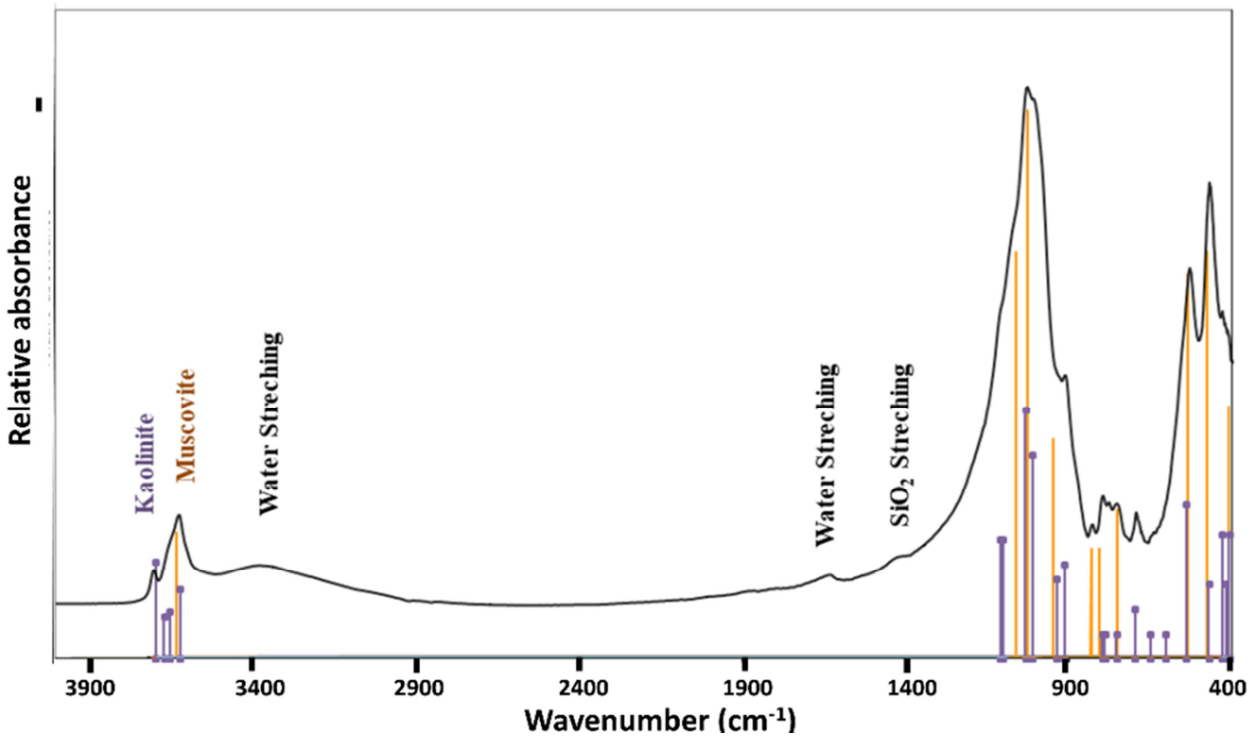

Figure-3: FTIR spectra of NGC

B. Effect of initial pH of the solution on MO adsorption in batch system

Preliminary equilibrium time experiments showed that the equilibrium adsorption time was 200 minutes. One of the essential constituent to control the rate of adsorption process that affect the surface charge of the adsorbent and the stability of the dye also is the pH of the solution mixture [15]. The effect of pH on the adsorption capacity of NGC for adsorption of MO were carried out at range of pH (3.0 to 9.0) for an initial concentration of 100 mg L^{-1} and 0.1 g of NGC in 50 mL of solution (Figure: 4). The results observed for the adsorption of MO on NGC surface was higher in the acidic medium and the adsorption capacity of the NGC toward MO decreases as the initial pH of the solution increases. Hence, the variation of initial pH leads to the variation of adsorption capacity of the clay in two possible mechanisms. Variation of pH affect the surface properties of the adsorbent. On the other hand, leads to variation in the degree of ionization of the adsorbate molecules [16]. At low pH there is an electrostatic attraction between positive surface charges of adsorbent and anionic dye (negative charge MO molecules). Moreover, increasing pH conduct the adsorbent surface charge to a negative charge and reduce the attraction force [17]. Furthermore, the pK_a of MO is 3.46, if pH of solution smaller than pK_a of MO the form of MO tended to be ionic, then it is easy to adsorb on the adsorbent with charge [18].

The pH at which the surface charge of adsorbent is zero called point of zero charge (pzc). Point of zero charge can be used to assess the ability of surface and type of surface active centers of the adsorbent [2]. Zero point of charge for NGC was determined at pH = 6.5. Where $pH > pH_{pzc}$ cationic dye adsorption is favored and where $pH < pH_{pzc}$ anionic dye adsorption take place [2].

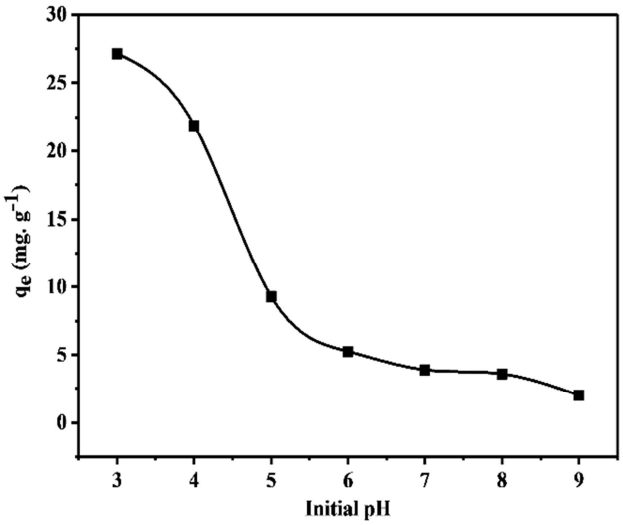

Figure-4: Effect of initial pH on the adsorption of MO on NGC

C. *Effect of adsorbent dosage in batch system*

Different amounts of the adsorbent (NGC) was used to determine its effect on the MO adsorption in the range between 0.4–4.0 g L^{-1} (V= 50 mL, C_o= 100 mg L^{-1} of MO, pH 3.0 and 6 hours shaking time) (Figure:5). The removal% increases from 29.6% to 66.4% for an increase of NGC dosage from 0.4 to 4.0 g L^{-1}. This increase may be attributed to the availability of a larger number of active adsorption sites toward MO molecules [19]. The adsorption capacity reduced from 74.0 to 16.6 mg g^{-1} as the NGC dosage increased from 0.4 to 4.0 g L^{-1} NGC. That is related to decrease in total adsorbent surface area as a result of cluster combination of adsorption sites [20].

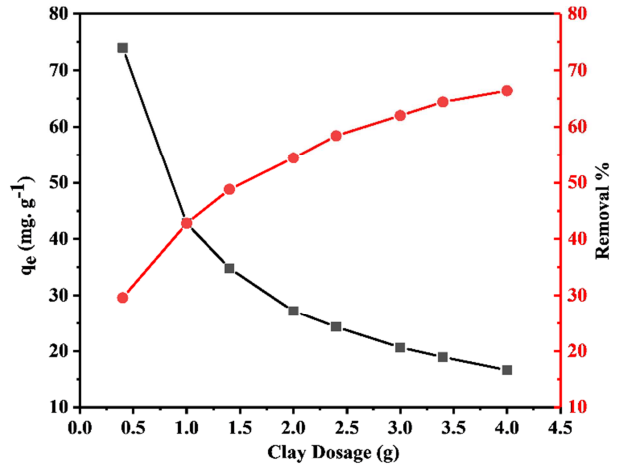

Figure-5: Effect of adsorbent dose on the adsorption of MO on NGC

D. *Effect of contact time and initial concentration*

The effect of contact time for adsorption process were carried out in concentration range of (10 to 150 mg L^{-1}) for the adsorbent dose of (2 g L^{-1}) at 303K. (Figure: 6-a) shows that at the first 25 minute, a rapid adsorption of MO takes place. Thereafter, the adsorption rate slow down and reach the equilibrium after 300 minute. This due to abundance of large surface area and surface adsorption sites at the begging. The rate of adsorption decreases with time due to the decrease of adsorption sites. Furthermore, the adsorbed MO transported from the external sites to the interior sites or pores [21].

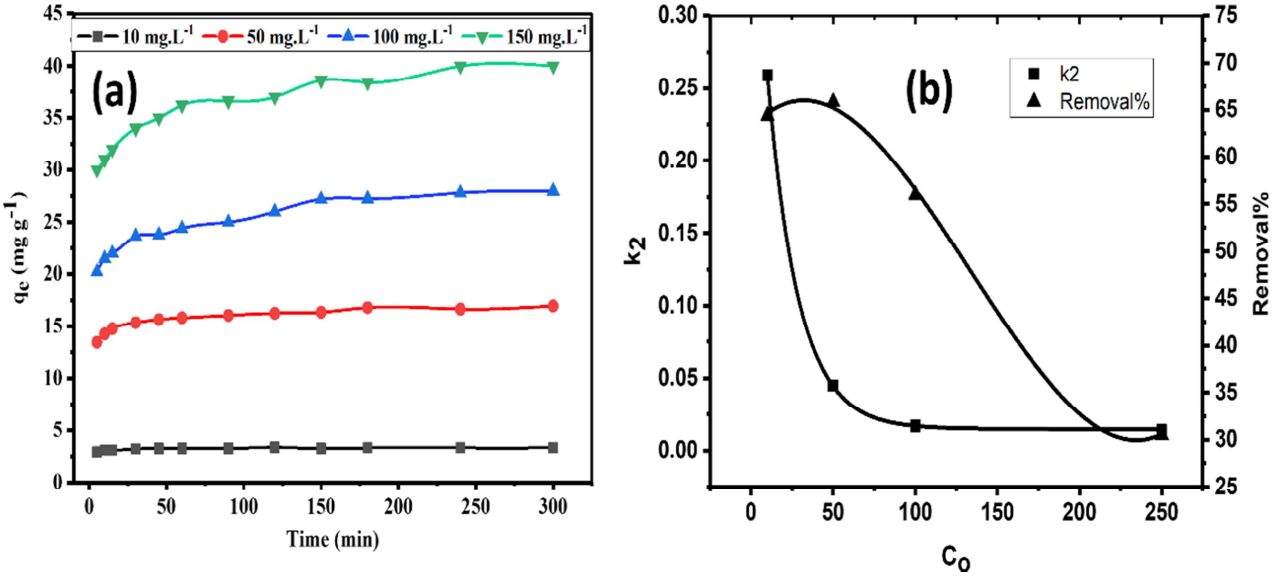

Figure-6: Equilibrium time study of different initial concentration of MO (a) and effect of initial concentration of MO on k_2 and removal% (b)

As shown in (**Error! Reference source not found.**-a), from the experimental data, it was observed that the adsorption capacity of MO increased as the initial dye concentration increases. This related to the more abundance of MO molecules in the solution which resulted in more driving force to dealing with the mass transfer resistance between the solid phase and aqueous phase [22].

E. Batch adsorption isotherms

The adsorption isotherm plays an important role to describe the adsorption system. The equilibrium relationship between adsorbent surface and adsorbate and maximum adsorption capacity can be measured using adsorption isotherms [23]. Langmuir and Freundlich Isotherms are two commonly used models used to understand the dye-clay interaction.

Langmuir isotherm (Eq. 9) is an empirical model based on the assumption of formation saturated monolayer at the maximum adsorption with one molecule in thickness over the homogeneous surface with constant enthalpy for each adsorbate molecule and sorption activation energy [24, 25].

$$q_e = \frac{q_m K_L C_e}{1+K_L C_e} \qquad (9)$$

Where q_e (mg g^{-1}) is the adsorption capacity of adsorbent at equilibrium, C_e (mg L^{-1}) is the adsorbate concentration at equilibrium, q_m (mg g^{-1}) is maximum monolayer coverage capacity and K_L (L mg^{-1}) is the Langmuir isotherm constant (Figure: 7-a).

The R_L factor could be calculated based on the (K_L) Langmuir constant given in (Eq. 10). The value of R_L indicates weather the adsorption process unfavorable if (R_L >1), favorable if (0<R_L <1), linear if (R_L =1), or irreversible if (R_L =0).

$$R_L = \frac{1}{1+K_L C_o} \qquad (10)$$

Freundlich isotherm (Eq. 11) is used to describe multilayer adsorption (Figure: 7-a). The underlying assumption is that adsorption sites are not equivalent and, hence, adsorption occurs first on stronger binding sites [25].

The equation expression can be represented as

$$q_e = K_F C_e^{\frac{1}{n}} \qquad (11)$$

Where K_F is Freundlich isotherm constant related to bonding energy, *1/n* value is related to adsorption intensity and *n* is the heterogeneity factor.

Temkin isotherm (Eq. 12) is characterized by a uniform binding energies. It assumes that the heat of adsorption of all molecules in the layer would decrease linearly rather than logarithmic with coverage (Figure: 7-b).

$$q_e = B \ln A_T C_e \qquad (12)$$

A_T is the Temkin isotherm equilibrium binding constant (L mg^{-1}) that indicate the adsorbent-adsorbate interaction, the constant $B=RT/b_T$ related to the heat of adsorption, R is the universal gas constant (8.314 J mol^{-1} K^{-1}), T is temperature in (K), and b_T is Temkin isotherm constant.

The isotherm parameters such as K_L, q_m, K_F and $1/n$ were determined using non-linear regression (

Table-1). It can be observed that the value of R_L is in between 0 and 1, that indicates the favorable adsorption of MO. The Freundlich isotherm constant ($1/n$) value is smaller than 1, which confirms a favorable adsorption process [26]. The decreasing value of Temkin constant (b_T) with increasing temperature shows that the adsorption is more favorable at high temperature due to its endothermic nature. The results for Langmuir isotherm model showed that the non-linear regression better fits to the experimental data according to the correlation coefficients (R^2) and the sum of square residual (SSE) values rather than Freundlich model fitting, conforming that the adsorption of MO on NGC as a monolayer adsorption.

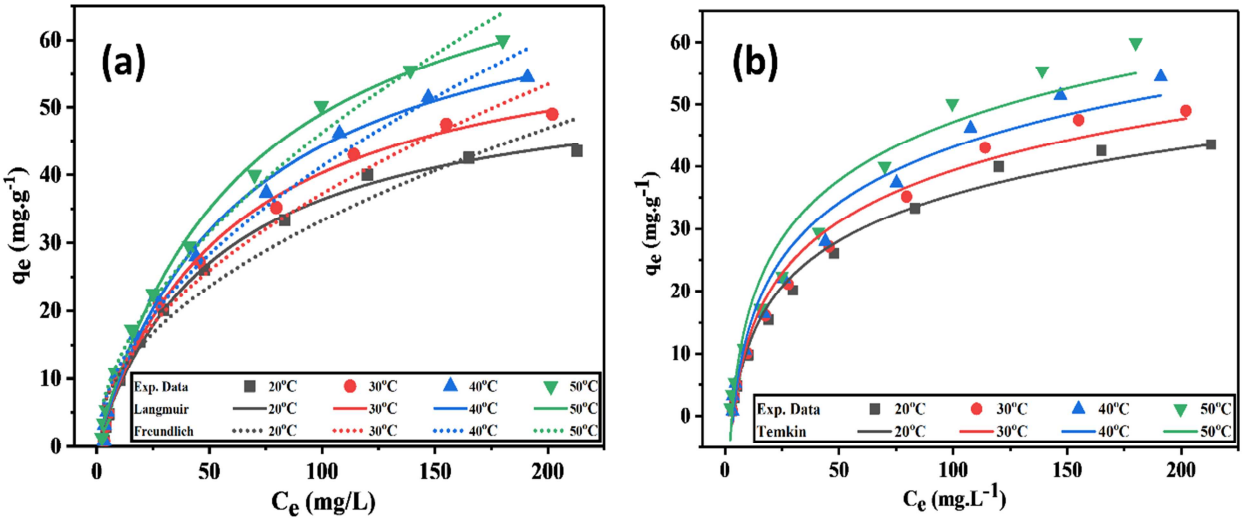

Figure-7: Non-linear fitting of Langmuir and Freundlich (a) Temkin isotherms (b) to the experimental data.

Table-1: Isotherm parameters for MO adsorption

		Temperature (K)			
Isotherm models	***Parameters***	***293***	***303***	***313***	***323***
Langmuir	q_m (mg g^{-1})	55.5	63.9	73.1	82
	K_L (L mg^{-1})	0.0190	0.0171	0.0154	0.0149
	R_L (C_o=100 mg L^{-1})	0.34	0.37	0.39	0.40
	R^2	0.996	0.995	0.995	0.996
	SSE	11.2	16.2	20.7	17.2
Freundlich	K_F (mg g^{-1})(L mg^{-1})	3.407	3.370	3.370	3.363
	$1/n_F$	0.495	0.552	0.544	0.553
	R^2	0.958	0.969	0.977	0.983
	SSE	110.63	102.66	90.34	77.48
	B	10.64	11.89	12.89	13.49
	b_T (kJ mole^{-1})	228.9	211.9	201.8	199.0
Temkin	A_T (L mg^{-1})	0.28	0.27	0.28	0.33
	R^2	0.988	0.984	0.975	0.960

SSE	32.1	52.1	97.5	187.4

F. Batch adsorption Kinetic Study

The mechanism of adsorption and characteristic constants of adsorption can be studied through kinetic measurements using pseudo first order, pseudo second order, and intra-particle diffusion.

Lagergren"s pseudo-first-order model is given as [27].

$$\frac{dq}{dt} = k_1(q_e - q_t) \qquad (13)$$

where q_e and q_t (mg g^{-1}) are the amounts of the MO adsorbed at equilibrium and at time t (min). k_1 (min^{-1}) is the rate constant (Figure: 8-a).

Pseudo-second-order kinetic model assumes that the rate of adsorption is second order with respect to the active surface sites [28].

$$\frac{dq}{dt} = k_2(q_e - q_t)^2 \qquad (14)$$

Where, k_2 is pseudo-second-order rate constant (Figure: 8-a). (Table: 3) shows the kinetic parameters at different temperatures (293, 303, 313 and 323 K) which were obtained from non-linear regression of the isotherm models.

The intra-particle diffusion model (Morris-Weber equation) is expressed as (Eq. 15).

$$q_t = k_{id}t^{0.5} + I \qquad (15)$$

Where, k_{id} is intra-particle diffusion constant (mg g^{-1} $min^{-0.5}$), I give information about thickness of the boundary layer. (Figure: 8-b) shows the plot of the applied intra-particle diffusion model to the experimental data. Two linear part of the plots were obtained with different slopes (Table: 3) that suggest a two-step mechanism for the adsorption of MO on NGC. A relatively fast sorption of MO on the exterior surface of NGC to saturation for the first step, followed by the intra-particle diffusion in the second step [29].

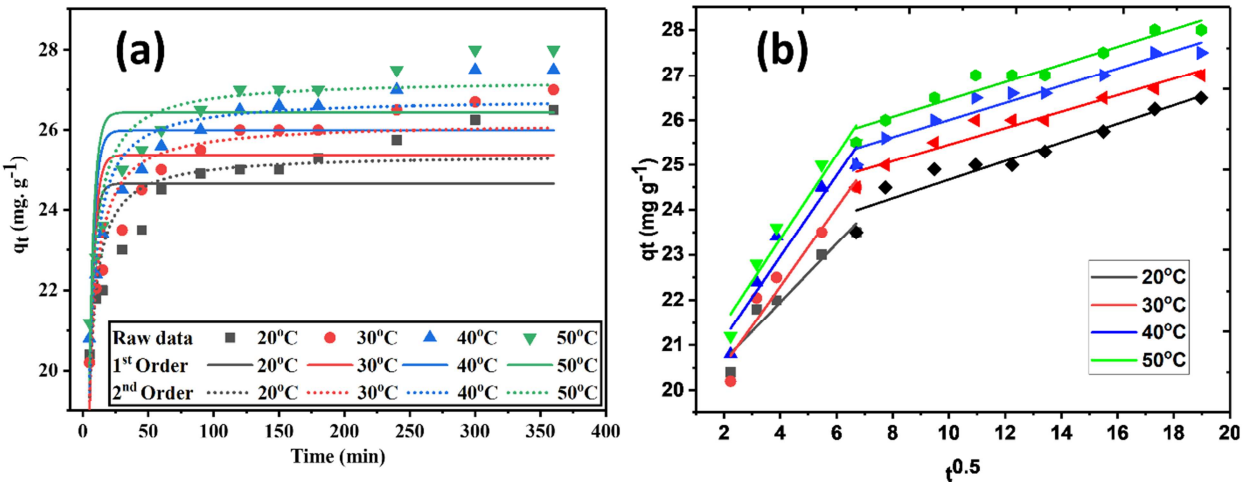

Figure-8: Pseudo first-order and pseudo second-order kinetic models (a) intra-particle diffusion model (b) applied to the experimental kinetic data for the adsorption of MO at different temperatures

It can be seen that the correlation coefficients (R^2 <0.602) for the first order kinetic model fitting are low and the *SSE* values are high while the second-order model fits well to the experimental data (Lower *SSE* values and higher R^2). In addition, the calculated (q_e) were adequately agree with the experimental data ($q_{exp.}$). The calculated (q_e) increases with increasing temperature and the rate constants varied with small value. Suggested that limiting steps may be physisorption through interaction between clay surface and MO molecules.

Table-3: The kinetic parameters from pseudo first-order, pseudo second-order and intra-particle diffusion models

		Temperature (K)			
Kinetic models	***Kinetic Parameters***	***293***	***303***	***313***	***323***
Experimental	q_{exp} (mg g^{-1})	26.25	27	27.5	28
Pseudo-First-Order	q_{calc} (mg g^{-1})	24.65	25.37	25.99	26.43
	k_1 (min^{-1})	0.3064	0.272	0.2745	0.2748
	R^2	0.480	0.581	0.603	0.590
	SSE	21.8	21.8	20.3	21.8
Pseudo-Second-Order	q_e (mg g^{-1})	25.4	26.2	28.8	27.3
	k_2 (g mg^{-1} min^{-1})	0.025	0.021	0.021	0.020
	R^2	0.825	0.895	0.910	0.905
	SSE	7.3	5.5	4.6	5.0
Intra-particle diffusion	K_{id}	0.21	0.18	0.19	0.19
	I	22.6	23.6	24.1	24.5
	R^2	0.963	0.968	0.969	0.971
	SSE	0.49	0.33	0.34	0.33

G. Thermodynamic Parameters

The thermodynamic parameters such as Gibbs free energy (ΔG^o), entropy (ΔS^o) and enthalpy (ΔH^o) for the adsorption of MO on NGC were calculated from the variation of K_c with temperature

Change of adsorption can be determined from the following equations [23].

$$\Delta G^o = \Delta H^o - T\Delta S^o \quad (16)$$

$$\Delta G^o = -RT \ln K_C \quad (17)$$

$$K_C = \frac{C_{Ae}}{C_e} \quad (18)$$

$$\ln K_C = \frac{\Delta S^o}{R} - \frac{\Delta H^o}{RT} \quad (19)$$

Where, ΔG^o is the free energy change (kJ mole^{-1}), ΔH^o is the enthalpy change (kJ mole^{-1}), and ΔS^o is the entropy change (kJ mole^{-1}). K_C, C_{Ae} and C_e, are the equilibrium constant, the amount of MO adsorbed on NGC at equilibrium (mg L^{-1}) and the equilibrium concentration of MO remain in solution (mg L^{-1}) respectively. The thermodynamic parameters are tabulated in (Table: 4). The positive value of ΔH^o indicates the endothermic adsorption of MO on NGC. The negative values of ΔG^o ensures the spontaneous nature of the adsorption of MO On the other hand, positive values of ΔG^o were obtained for high MO concentration (200 mg L^{-1}). This may be due to the competition between MO molecules at higher concentrations which result in the decrease of spontaneity of the process.

Table-4: Thermodynamic parameters

Dye concentration (mg. L^{-1})	***ΔH^o (KJ. Mole^{-1})***	***ΔS^o (KJ. Mole^{-1})***	***ΔG^o (KJ. Mole^{-1})***			
			293 K	***303 K***	***313 K***	***423 K***
30	8.87	0.04	-1.55	-1.91	-2.27	-2.62
50	7.93	0.03	-1.17	1.48	-1.79	-2.1
100	7	0.02	-0.2	-0.44	-0.69	-0.93
200	10.75	0.03	1.02	0.68	0.35	0.02

H. Empirical modeling of breakthrough curves in fixed-bed Adsorption studies

The breakthrough curve can be obtained from plotting C_t (mg L^{-1}) or C_t/C_o vs V_{eff} (mL) or t (min). Where C_o and C_t are the influent and effluent concentrations respectively. V_{eff} is the treated volume of effluent solution, t is the process time. V_{eff} can be determine as:

$$V_{eff} = Qt \quad (20)$$

Where Q is influent flow rate (mL min^{-1}) and t is consumption time (min).

The fixed-bed capacity (q_{total}) (mg) for a significant influent MO concentration C_o and influent flow rate Q is equal to the computational determination of the area under the curve achieved from integrating the adsorbent concentration which is expressed as C_{ad} ($C_{ad} = C_o - C_t$) at a given time t (min) [30]. q_{total} can be calculated as:

$$q_{total} = \frac{QA}{1000} = \frac{Q}{1000}\int_{t=0}^{t=t_{total}} C_{ad}\,dt \quad (21)$$

Where A is the area under the plot, t_{total} is the total flow time. Equilibrium uptake q_{eq} (mg g^{-1}) can be determined using (Eq. 22):

$$q_{eq(\exp)} = \frac{q_{total}}{m} \quad (22)$$

Where m is the mass of clay granule in the column (g), the amount of adsorbed MO which passed through the column can be determine as W_{total}:

$$W_{total} = \frac{C_0 Q t_{total}}{1000} \quad (23)$$

The percentage of adsorbed MO in column can be determine as $R\%$ (Eq. 24):

$$R\% = \frac{q_{total}}{W_{total}} \times 100 \quad (24)$$

I. Effect of Calcining temperature and granule particle size

The breakthrough curves for the adsorption of MO on natural Garmk clay granules (NGG) at different calcining temperatures and different granule particle size are shown in (Figure: 9-a and 9-b) (flow rate= 5 mL min^{-1}, room temp., initial concentration of MO= 50 mg g^{-1}) with the applied kinetic models (Thomas and Yoon Nelson). (Table: 5) presents the kinetic parameters calculated from non-linear regression of Thomas and Yoon-Nelson models. The results show that 550 °C calcination temperature give highest q_{total} value at which the texture is fixed without further sintering of the clay particles that may reduce the adsorption capacity.

The breakthrough curves for the effect of particle size of NGG granules on the adsorption capacity (Figure: 9-b) shows that as the particle size of the granules increases the required time for the breakthrough points decreases as a result of decreasing the surface area of the granule which affect the mass transfer of MO between the bulk solution and the surface of the clay granules. The maximum adsorption capacity (q_{total}) were at smaller size within this study (Table: 5).

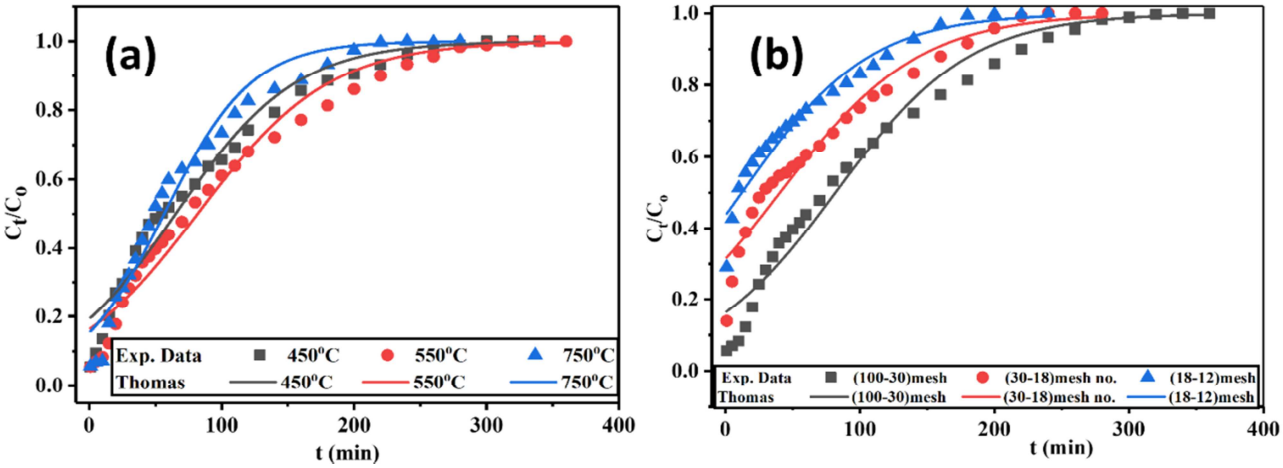

Figure-9: Effect of calcination temperature (a) and the granules particle size (b) on the breakthrough curves for the adsorption of MO on NGG

J. *Effect of experimental conditions*

Different experimental conditions such as flow rate, bed height, and initial MO concentration were investigated (room temperature, 100-30 mesh granules, 550 °C calcining temperature. As the flow rate of the influent solution increase the breakthrough point time shifted towards shorter time (Figure: 10-a). The breakthrough point is the time at which the ratio of effluent concentration to the influent concentration (C_t/C_o=0.05) [30]. At a flow rate of 3 mL min^{-1} the value of (C_t/C_o) reach 0.05 after 10 minutes. However, for both (5 and 7 mL min^{-1}) the breakthrough time is less than 1 minute due to the retention time require to adsorb MO on the granule surface and mass transfer between bulk solution and granule surface [31]. In addition, a much sharper breakthrough curve obtained at lower flow rate due to increasing flow rate leading to reduce diffusion time of MO molecules into the NGG for sorption [30]. The column capacity for adsorption (q_{total}) increases as the flow rate increased as a result of higher influent MO concentration loading in to the column at higher flow rates.

Increasing of the bed height in the column leads to the increase in contact time between NGG particles and MO during the process It was observed that as the bed height of the column decreases the breakthrough point shifts toward shorter time as a result of reducing of contact time for sorption (Figure: 10-b) [32]. The value of q_{total} increases as the bed height increased which may be due to increasing the active sites and surface area of NGG at higher bed heights.

The initial concentration of MO had a significant effect on the breakthrough point and exhausting time (Figure: 10-c). Steeper breakthrough curves were obtained as the initial concentration of MO increased. This may be due to lower mass-transfer flux from the MO in the solution to the granule surface and weaker driving force [30]. The adsorption capacity (q_{total}) of the column increases with increasing the initial MO concentration due to the increase of dye loading rate as a result of increasing influent concentration [33].

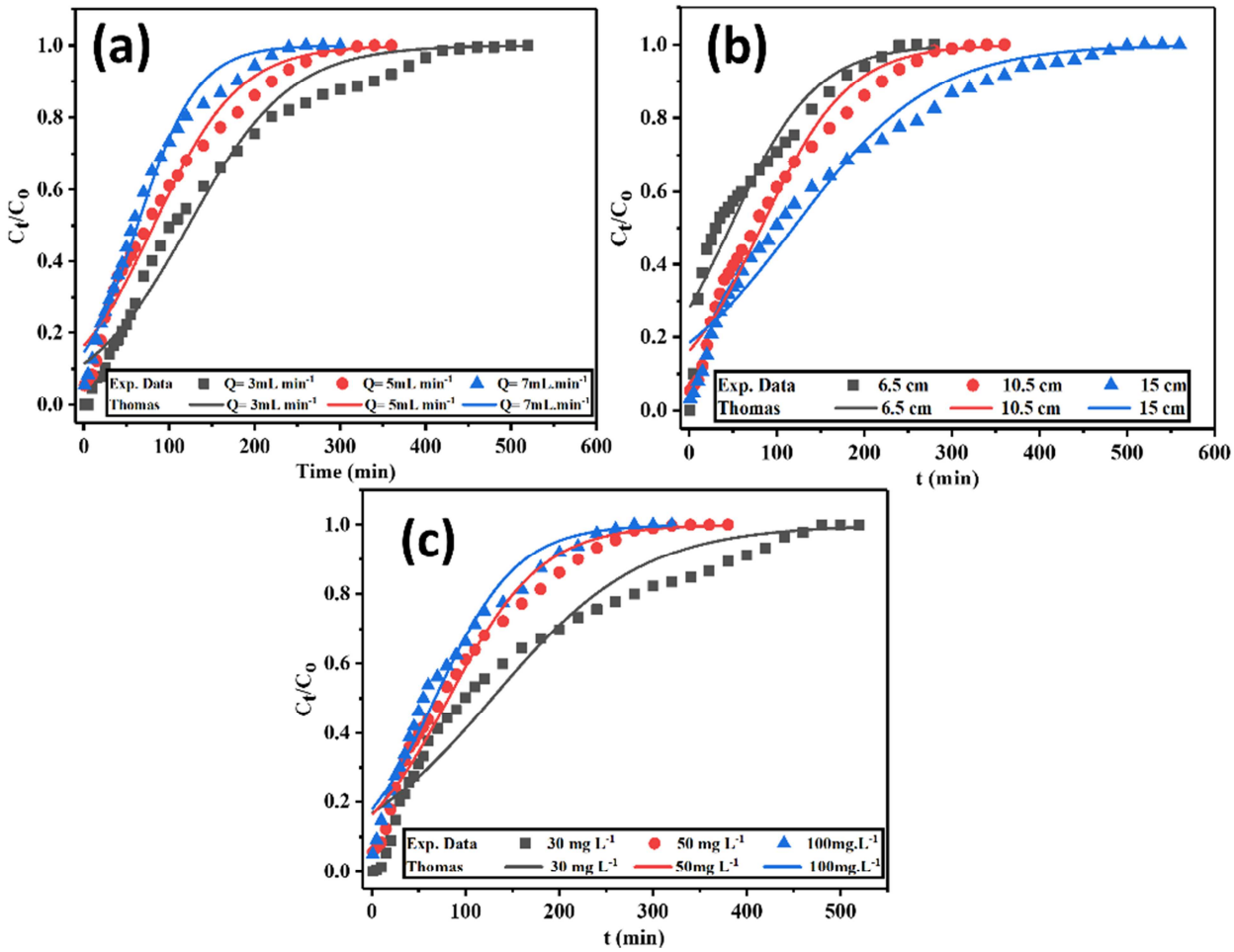

Figure-10: Effect of influent flow rate (a) granules bed height (b) and initial MO concentration (c) on the adsorption of MO on NGG

Table-5: Effect of calcining temperature, granules particle size, flow rate, bed height and initial MO concentration on the adsorption of MO C_o (mg L^{-1})

C_o (mg L^{-1})	Bed height (cm)	Flow rate (mL min^{-1})	Granule size (mesh no.)	Calcining temp. (^oC)	q_{total} (mg)	R%
50	10.5	5	0.2-0.6	450	3.34	4.45
50	10.5	5	0.2-0.6	550	4.17	4.91
50	10.5	5	0.2-0.6	750	3.93	5.62
50	10.5	5	0.6-1.0	550	2.64	4.40
50	10.5	5	1.0-1.7	550	2.14	4.28
50	10.5	3	0.2-0.6	550	1.82	2.43
50	10.5	7	0.2-0.6	550	5.89	6.48
50	6.5	5	0.2-0.6	550	3.30	5.08
50	15.0	5	0.2-0.6	550	4.64	3.57
30	10.5	5	0.2-0.6	550	2.77	3.85
100	10.5	5	0.2-0.6	550	8.92	6.37

K. Kinetic modelling of breakthrough curves

Tomas model is an alternative form of the Bohart-Adams model (Eq. 25) [27]. The Thomas model assumption is that the adsorption process follows the Langmuir kinetics with no axial dispersion, and their constant separation factor could be applicable to both favorable and unfavorable isotherms [33].

$$\ln\left(\frac{C_o}{C_t}-1\right)=\frac{K_{BA}N_0Z}{u}-K_{BA}C_ot \qquad (25)$$

Where, K_{BA} is Bohart-Adams rate constant ($cm^3\ mg^{-1}\ min^{-1}$), N_o is adsorption capacity per unit volume of sorbent bed ($mg\ cm^{-3}$), and u is influent velocity ($cm\ min^{-1}$).

The non-linear form for Thomas model equation is given as [33].

$$\frac{C_t}{C_o}=\frac{1}{1+e^{[K_{TH}(\frac{q_om-C_oV_{eff}}{Q}]}} \qquad (26)$$

K_{TH} is the Thomas rate constant ($mL\ mg^{-1}\ min^{-1}$), q_o is the equilibrium adsorbate uptake ($mg\ g^{-1}$), m is the mass of adsorbent in the column (g). C_o is the initial concentration of influent MO ($mg\ L^{-1}$), C_t is effluent MO concentration ($mg\ L^{-1}$), Q is the flow rate ($mL\ min^{-1}$), and V_{eff} is the effluent volume (mL).

The kinetic parameters of Thomas model were estimated from the non-linear curve fitting of the experimental data using OriginPro 9.0. For the different experimental conditions (Granule calcining temperature, granule particle size, flow rate, bed height and initial MO concentration) the breakthrough curves according to the Thomas model (Figure: 9-10) and the kinetic parameters are listed in Table 6.

Thomas rate constant increased with increasing granule particle size while the value of (q_o) decreased. Increasing the flow rate from 3 to 7 $mL\ min^{-1}$, the K_{TH} value increases from 3.4×10^{-4} to 5.6×10^{-4} ($mL\ min^{-1}\ mg^{-1}$), and q_o increases from 723 to 890 $mg\ g^{-1}$due to the increasing in total number of MO molecules diffused in to the pores and the surface of the granule.

Lower K_{TH} observed with increasing the granules bed height which results from the longer contact time of the adsorbent for adsorption, while q_o increases with bed height because the total number of the active sites has increased [34]. Continuous MO uptake process is also affected by the MO influent concentration as listed in (Table 6). The K_{TH} value decrease with increasing influent MO concentration, however, q_o increases relative to the driving force which makes the column run more efficiently due to increasing in MO concentration [35]. The value of square correlation coefficients (R^2) form non-linear regression of Thomas model as listed in Table 6 shows a good fitting with all experimental data that investigated in this study.

Table-6: Thomas kinetic model parameters at different experimental conditions

Thomas parameters	*calcining temp. (^oC)*			*Granule size (mesh no.)*			*Flow rate ($mL.min^{-1}$)*			*Bed Height (cm)*			*Initial MO concentration ($mg.\ L^{-1}$)*		
	450	550	750	70-30	30-18	18-12	3	5	7	6	10.5	15	30	50	100
K_{TH} (10^{-4} mL min^{-1} mg^{-1})	4.4	4	6	4	3.8	4.2	3.4	4	5.6	4.08	4.01	2.6	4.33	4.01	1.53
q_o (mg/g)	650	820	570	820	410.5	123.8	723.5	820	890	768	817	818	738.5	818	1330
R^2	0.97	0.974	0.969	0.974	0.957	0.955	0.974	0.974	0.984	0.900	0.974	0.967	0.94	0.974	0.967

L. Conclusion

The adsorption of MO from aqueous solution based on low-cost adsorbent (natural Garmk clay NGC, and natural Garmk clay Granules (NGG) was investigated in batch and continuous systems. For the batch system, the adsorption kinetic was satisfied with pseudo-second order kinetic model with q_e =26.1 mg L^{-1} at 303K. Maximum adsorption capacity was at pH 3. The equilibrium data was best fit with Langmuir isotherm model at all temperatures. The thermodynamic parameters (ΔH^o, ΔS^o and ΔG^o) shows an endothermic, spontaneous adsorption at low concentrations. However, at high MO concentrations (200 mg L^{-1}) a non-spontaneous adsorption was detected.

For the fixed bed continuous system, the breakthrough curves were highly dependable on all operational parameters within this study. The best conditions for MO adsorption on NGG were obtained at smaller particle size, 550 ^oC granule calcining temperature, increased flow rate, higher bed, and higher influent MO concentration. The study shows that the Garmak natural clay can be used as an efficient and low cost adsorbent for the treatment of wastewater polluted with anionic dye like MO and other anionic dyes. The results of this work can be beneficial for the environmental pollution prevention in industries that use dye in the finishing step as well as medical and biological laboratories that use stains in bacterial identifications (blood film preparation).

References

[1] Y. Omidi, R. Heydari, and H. Nourmoradi, Hesam Basiri, Hassan Basiri, *"Low-cost sorbent for the removal of aniline and methyl orange from liquid-phase: Aloe Vera leaves wastes"*, J. Taiwan Inst. Chem. Eng.,Vol. 68, pp. 90–98, (2016).

[2] M. T. Yagub, T. K. Sen, S. Afroze, and H. M. Ang, *"Author " s personal copy Dye and its removal from aqueous solution by adsorption : A review"*, Adv. Colloid Interface Sci., Vol. 209, pp. 172–184, (2014).

[3] Z. X. Chen, X. Y. Jin, Z. Chen, M. Megharaj, and R. Naidu, *"Removal of methyl orange from aqueous solution using bentonite-supported nanoscale zero-valent iron"*, J. Colloid Interface Sci., Vol. 363, No. 2, pp. 601–607, (2011).

[4] T. A. Khan, R. Rahman, and E. A. Khan, *"Adsorption of malachite green and methyl orange onto waste tyre activated carbon using batch and fixed-bed techniques: isotherm and kinetics modeling"*, Model. Earth Syst. Environ., Vol. 3, No. 1, (2017).

[5] A. A. Adeyemo, I. O. Adeoye, and O. S. Bello, *"Adsorption of dyes using different types of clay: a review"*, Appl. Water Sci., Vol. 7, No. 2, pp. 543–568, (2017).

[6] T. Robinson, B. Chandran, and P. Nigam, *"Removal of dyes from a synthetic textile dye effluent by biosorption on apple pomace and wheat straw"*, Water Res., Vol. 36, No. 11, pp. 2824–2830, (2002).

[7] O. S. Bello, M. A. Ahmad, and N. Ahmad, *"Adsorptive features of banana (Musa paradisiaca) stalk-based activated carbon for malachite green dye removal"*, Chem. Ecol., Vol. 28, No. 2, pp. 153–167, (2012).

[8] K. Y. Foo and B. H. Hameed, *"Value-added utilization of oil palm ash: A superior recycling of the*

industrial agricultural waste", J. Hazard. Mater., Vol. 172, No. 2–3, pp. 523–531, (2009).

[9] M. T. Yagub, T. K. Sen, and H. M. Ang, *"Equilibrium, kinetics, and thermodynamics of methylene blue adsorption by pine tree leaves"*, Water. Air. Soil Pollut., Vol. 223, No. 8, pp. 5267–5282, (2012).

[10] V. Vadivelan and K. Vasanth Kumar, *"Equilibrium, kinetics, mechanism, and process design for the sorption of methylene blue onto rice husk"*, J. Colloid Interface Sci., Vol. 286, No. 1, pp. 90–100, (2005).

[11] N. M. Mahmoodi, M. Arami, H. Bahrami, and S. Khorramfar, *"Novel biosorbent (Canola hull): Surface characterization and dye removal ability at different cationic dye concentrations",* Desalination, Vol. 264, No. 1–2, pp. 134–142, (2010).

[12] Y. Chen and M. Wang, *"Removal of Crystal Violet and Methylene Blue from Aqueous Solution using Soil"*, Int. Conf. Environ. Sci. Eng., Vol. 8, pp. 252–254, (2011).

[13] M. K. Uddin, *"A review on the adsorption of heavy metals by clay minerals, with special focus on the past decade",* Chem. Eng. J., Vol. 308, pp. 438–462, (2017).

[14] R. Elmoubarki *et al.*, *"Adsorption of textile dyes on raw and decanted Moroccan clays: Kinetics, equilibrium and thermodynamics"*, Water Resour. Ind., Vol. 9, pp. 16–29, (2015).

[15] M. V. Subbaiah and D. S. Kim, *"Adsorption of methyl orange from aqueous solution by aminated pumpkin seed powder: Kinetics, isotherms, and thermodynamic studies"*, Ecotoxicol. Environ. Saf., Vol. 128, pp. 109–117, (2016).

[16] B. K. Nandi, A. Goswami, and M. K. Purkait, *"Removal of cationic dyes from aqueous solutions by kaolin: Kinetic and equilibrium studies"*, Appl. Clay Sci., Vol. 42, No. 3–4, pp. 583–590, (2009).

[17] A. Kausar *et al.*, *"Dyes adsorption using clay and modified clay: A review"*, J. Mol. Liq., Vol. 256, pp. 395–407, (2018).

[18] Q. Ma, F. Shen, X. Lu, W. Bao, and H. Ma, *"Studies on the adsorption behavior of methyl orange from dye wastewater onto activated clay"*, Desalin. Water Treat., Vol. 51, No. 19–21, pp. 3700–3709, (2013).

[19] T. M. Albayati, G. M. Alwan, and O. S. Mahdy, *"High performance methyl orange capture on magnetic nanoporous MCM-41 prepared by incipient wetness impregnation method"*, Korean J. Chem. Eng., Vol. 34, No. 1, pp. 259–265, (2017).

[20] R. Huang, Q. Liu, J. Huo, and B. Yang, *"Adsorption of methyl orange onto protonated cross-linked chitosan"*, Arab. J. Chem., Vol. 10, No. 1, pp. 24–32, (2017).

[21] V. S. Munagapati, V. Yarramuthi, and D. S. Kim, *"Methyl orange removal from aqueous solution using goethite, chitosan beads and goethite impregnated with chitosan beads"*, J. Mol. Liq., Vol. 240, pp. 329–339, (2017).

[22] M. Duhan and R. Kaur, *"Adsorptive removal of methyl orange with polyaniline nanofibers: an unconventional adsorbent for water treatment"*, Environ. Technol. (United Kingdom), pp. 1–34, (2019). https://doi.org/10.1080/09593330.2019.1593511

[23] J. Zhang, Q. Zhou, and L. Ou, *"Kinetic, isotherm, and thermodynamic studies of the adsorption of methyl orange from aqueous solution by chitosan/alumina composite"*, J. Chem. Eng. Data, Vol. 57, No. 2, pp. 412–419, (2012).

[24] Aishah A.Jalil, Sugeng Triwahyono, S. Hazirah Adam, N. DianaRahim, M. Arif, A. Aziz, N. Hanis, H.Hairom, N. Aini, M.RazaliMahani, A.Z.Abidin, M. Khairul, A.Mohamadiah., *"Adsorption of methyl orange from aqueous solution onto calcined Lapindo volcanic mud",* J. Hazard. Mater., Vol. 181, No. 1–3, pp. 755–762, (2010).

[25] K. Y. Foo and B. H. Hameed, *"Insights into the modeling of adsorption isotherm systems"*, *Chem. Eng. J.*, Vol. 156, No. 1, pp. 2–10, (2010).

[26] M. K. Sahu and R. K. Patel, *"Using modi fi ed red mud : kinetics and equilibrium",* RSC Adv., Vol. 5, pp. 78491–78501, (2015).

[27] K. L. Tan and B. H. Hameed, *"Insight into the adsorption kinetics models for the removal of contaminants from aqueous solutions"*, J. Taiwan Inst. Chem. Eng., Vol. 74, pp. 25–48, (2017).

[28] A. Aurich *et al.*, *"Improved Isolation of Microbiologically Produced (2R,3S)-Isocitric Acid by Adsorption on Activated Carbon and Recovery with Methanol"*, Org. Process Res. Dev., Vol. 21, No. 6,

pp. 866–870, (2017).

[29] H. R. Ahmed, S. J. Raheem, and B. K. Aziz, *"Removal of Leishman stain from aqueous solutions using natural clay of Qulapalk area of Kurdistan region of Iraq"*, Karbala Int. J. Mod. Sci., Vol. 3, No. 3, pp. 165–175, (2017).

[30] H. Demey-Cedeño, M. Ruiz, J. A. Barron-Zambrano, and A. M. Sastre, *"Boron removal from aqueous solutions using alginate gel beads in fixed-bed systems",* J. Chem. Technol. Biotechnol., Vol. 89, No. 6, pp. 934–940, (2014).

[31] M. Auta and B. H. Hameed, *"Chitosan-clay composite as highly effective and low-cost adsorbent for batch and fixed-bed adsorption of methylene blue"*, Chem. Eng. J., Vol. 237, pp. 352–361, (2014).

[32] T. M. Darweesh and M. J. Ahmed, *"Batch and fixed bed adsorption of levofloxacin on granular activated carbon from date (Phoenix dactylifera L.) stones by KOH chemical activation"*, Environ. Toxicol. Pharmacol., Vol. 50, pp. 159–166, (2017).

[33] M. T. Yagub, T. K. Sen, S. Afroze, and H. M. Ang, *"Fixed-bed dynamic column adsorption study of methylene blue (MB) onto pine cone"*, Desalin. Water Treat., Vol. 55, No. 4, pp. 1026–1039, (2015).

[34] N. Mohammed, N. Grishkewich, H. A. Waeijen, R. M. Berry, and K. C. Tam, *"Continuous flow adsorption of methylene blue by cellulose nanocrystal-alginate hydrogel beads in fixed bed columns"*, *Carbohydr. Polym.*, Vol. 136, pp. 1194–1202, (2016).

[35] S. Afroze, T. K. Sen, and H. M. Ang, *"Adsorption performance of continuous fixed bed column for the removal of methylene blue (MB) dye using Eucalyptus sheathiana bark biomass"*, Res. Chem. Intermed., Vol. 42, No. 3, pp. 2343–2364, (2016).